Int. J. Electrochem. Sci., 12 **(2017)** 9855 – 9864, doi: 10.20964/2017.10.23

International Journal of
ELECTROCHEMICAL
SCIENCE
www.electrochemsci.org

Short Communication

Anti-corrosion Properties of a Bioinspired superhydrophobic surface on Stainless Steel

Erling Zhao[1], *Yanqiang Li*[1], *Liguo Gao*[1,*], *Shuzhang Yang*[1], *Tingli Ma*[2,*]

[1]State Key Laboratory of Fine Chemicals, School of petroleum and chemical engineering, Dalian University of Technology, Panjin, 124221, China.
[2]Graduate School of Life Science and Systems Engineering, Kyushu Institute of Technology, Kitakyushu, Fukuoka, 808-0196, Japan
[*]E-mail: liguo.gao@dlut.edu.cn, tinglima@dlut.edu.cn

Received: 2 March 2017 / *Accepted:* 19 July 2017 / *Published:* 12 September 2017

Metal corrosion causes tremendous financial loss and disasters every year. Inspired by "lotus effect," a superhydrophobic stainless steel surface with anti-corrosion property was realized in this study. The bioinspired micro–nano structures were fabricated by utilizing two chemical etching procedures. The water contact angle (CA) of the prepared surface reached 173°. The correlative mechanism between CA and surface morphology was elucidated by adjusting the key reaction conditions. Electrochemical corrosion test showed that the bioinspired superhydrophobic stainless steel possessed a polarization resistance that is 28.9 times higher than that of common stainless-steel surface.

Keywords: Superhydrophobic; Stainless steel; Micro-nano structure; Anti-corrosion

1. INTRODUCTION

In recent years, bioinspired surfaces with superhydrophobicity have been intensively investigated and improved by discoveries of superwetting phenomena in nature, such as rose petals, lotus leaf, and gecko's feet. The superhydrophobic surfaces on these organisms refer to the surfaces with a static CA exceeding 150° [1,2]. Rose petals exhibit superhydrophobicity with high adhesion, which is related to periodic arrays of micropapillae covered by nanofolds [3,4]. The low adhesive, superhydrophobic, and self-cleaning properties of lotus leaf are due to its randomly distributed micropapillae covered by branch-like nanostructures [5]. Gecko's feet with superhydrophobic,

reversible adhesive, and self-cleaning functions are contributed by the aligned microsetae splitting into hundreds of nanospatulae [6].

At present, superhydrophobic surfaces have attracted considerable interest because of their satisfactory application in microfluidic devices [7], medical science [8], oil purification [9], oil/water separation [10,11], self-cleaning [12], anti-corrosion [13,14], and drag reduction [15]. Low surface free energy and appropriate surface feature are two important factors to fabricate surperhydrophobic surface [16].

Stainless steel is widely used in numerous fields, such as machinery manufacturing, ships, and aerospace owing to its excellent mechanical performance. However, stainless still will suffer corrosion when exposed to aggressive media. Therefore, how to enhance the anti-corrosion of metal materials has become a major research topic. The use of organic and polymeric protective coatings is an effective method for separating metallic surfaces from corrosive environments [17,18]. One of the most commonly used methods is the addition of alloying elements, which can atomically bind with metals. The behavior of the interfaces with the surrounding media or the surface properties can be improved without compromising the metal thermal or electromechanical properties. Among the elements, Cr is an effective element that has been added using a pre-treatment technology on stainless steel to achieve corrosion protection [19,20]. Despite the advantages of good performance and low cost, this traditional technology has been restricted because of the toxicity and carcinogenic nature of Cr [21]. Graphene oxide and graphene, which are either deposited or directly grown onto pre-formed surfaces, could prevent electrochemical corrosion [18,22]. Deyab studied the anti-corrosion effect of carbon nanotubes on carbon steel [23].

Compared with other technologies, chemical etching can be considered because of its economic advantage. Therefore, this work demonstrates chemical etching method to fabricate superhydrophobic surface inspired by "lotus effect." The functional superhydrophobic surface is fabricated on stainless steel via a two-step etching method; the first step involves the fabrication of micron pore structures, whereas the second step is patterning nano pits on these micro pore structures. The micro–nano structures are similar to the surface of lotus leaf, in which micropapillae were covered by branch-like nanostructures. The electrochemical corrosion characterization shows that the bioinspired superhydrophobic stainless steel surface possesses markedly higher polarization resistance (R_p) than common stainless-steel surface.

2. EXPERIMENTAL SECTION

2.1 Materials

The SUS304 stainless steel (chemical composition: 0.08 wt.% of C, 2.00 wt.% of Mn, 0.045 wt.% of P, 0.03 wt.% of S, 1.00 wt.% of Si, 18.0-20.0 wt.% of Cr, 8.0-10.5 wt.% of Ni, and the remaining element Fe) were obtained from commercial sources (Amanda, Shenzhen, China). Sodium chloride (Sinopharm Chemical Reagent Co., Ltd., China), hydrochloric acid (36.5%, Tianjin Damao, China), ethanol, phosphoric acid, hydrogen peroxide, acetic acid (AR, Tianjin Kemiou Chemical

Reagent Co., Ltd., China), Ferric chloride (AR, Tianjin Damao, China), chloroform, and acetone (AR, Beijing Chemical works, China) were purchased from commercial sources at the highest available purity and used without further purification. The deionized (DI) water used in the experiment was prepared by Dura 24FV (The-lab Co., Ltd., USA). 1H,1H,2H,2H-Perfluorodecyltriethoxysilane (PFDTES) were purchased from J & K Chemical Technology.

2.2 Preparation of Solution

Ferric chloride solution: $FeCl_3$ etching solution was prepared by dispersing 8.0 g $FeCl_3$ into 30 mL DI water. Then, 2 mL HCl (1 M), 2 mL H_3PO_4 (85 wt%), and 2 mL H_2O_2 (30 wt%) were poured into the above mentioned solution. The etching solution was stirred for 30 min with a glass rod.

PFDTES-ethanol solution: PFDTES-ethanol solution was obtained by adding PFDTES (0.3 g) in the ethanol solution (30 ml). Then trace glacial acetic acid was taken using the pipetting to adjust the pH of the solution about 4, which can inhibit Si-OH dehydration to produce Si-O-Si. The prepared solution was placed on a magnetic stirrer for 5 h to form a uniform and transparent liquid.

2.3 Fabrication of Superhydrophobic Stainless Steel Surface

Stainless steel with a thickness of 0.2 mm was cut into 2*2 cm^2 slices and washed in an ultrasonic bath with chloroform, acetone, ethanol, DI water for approximately 5 min, respectively. Then, they were dried under nitrogen gas flow. The samples were immersed into ferric chloride solution for about 4 min to fabricate micron pore structures. Then they were washed by DI water. To form nano pits, the samples were transferred into prepared HCl acid solution (1 M) for a certain period of time (15-20 min). Finally, superhydrophobic stainless steel surface was obtained after immersing the sheet into PFDTES-ethanol solutions for 30 min and curing in an oven at 80 ℃ for 15 min. We explored influences of $FeCl_3$ concentration, HCl concentration and etching time of HCl on hydrophobicity of the stainless steel surface (see supporting information from Figure S1 to Figure S3).

2.4 Characterization

Superhydrophobic properties were measured with a 5 μL DI water droplet by CA measurement (OCAH200, Dataphysics Instruments) with a CCD camera. The average CA value for the same sample was obtained by measuring more than three different positions. The morphologies were observed by scanning electron microscope (SEM) instrument (Nova NanoSEM 450, FEI). X-ray diffraction (XRD) was characterized by XRD-7000S (Shimadzu Corporation, Japan). UV-Vis diffuse reflectance spectroscopy (DRS) was characterized by the image of ultraviolet-visible spectrophotometer (Lambda 950). R_p ability was measured using an electrochemical workstation in a three electrode cell (CS310, CorrTest). A saturated calomel electrode and platinum wire was employed as the reference electrode and counter electrode, respectively. The potentiodynamic polarization curves for the stainless steel

with different CA in 3.5 wt% NaCl solution. The polarization curves were obtained with test sensitivity of 10^{-2} s and a scan rate of 1 mV/s.

3. RESULTS AND DISCUSSION

The generation of superhydrophobic stainless steel surface is schematically shown in Fig. 1. Significant surface wetting changes occurred after two-step chemical etching and surface energy modification. First, the microstructure surface of stainless steel was fabricated by using $FeCl_3$ etching solution. Subsequently, another etching procedure was applied to develop nanostructure on the microstructure surface. The superhydrophobic surface was obtained after the surface was modified with low-surface-energy molecules of PFDTES.

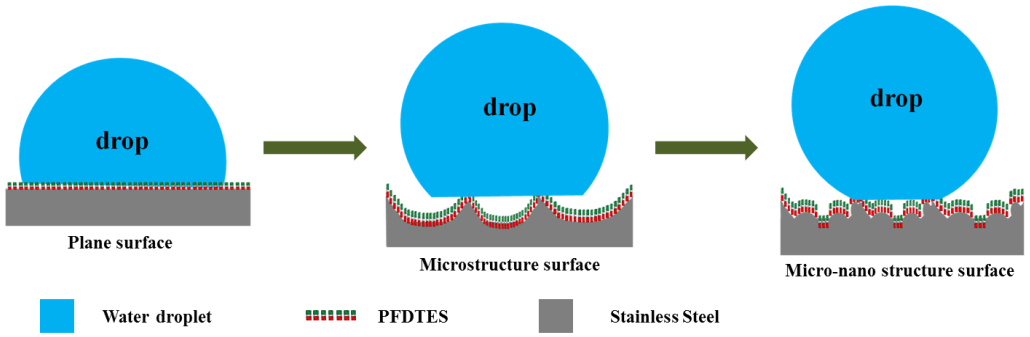

Figure 1. Scheme of the fabrication of bioinspired superhydrophobic surface on stainless steel substrate: the first step is to fabricate microstructure on the stainless steel surface; the second step is to pattern nanostructures on microstructure surface.

Fig. 2 shows CA test and SEM images collected during the fabrication of the bioinspired surface. All the samples possess assembled PFDTES. The CA of water droplets on the common stainless-steel surface was 114° shown in Fig. 2a. The surface was relatively smooth. Only some polishing scratches emerged on the surface (Fig. 2d). After the first-step etching by $FeCl_3$, the surface topographies of the samples differed from those of untreated samples, and the CA of water droplets on the stainless-steel surface increased to 146° as shown in Fig. 2b. The corresponding top-view SEM image is presented in Fig. 2e. A large quantity of uniformly micron pore structures (2–5 μm) on the surface of stainless steel was observed. The micron pore structures were relatively shallow, completely covering the stainless steel and thus increasing hydrophobicity via providing less contact area between stainless steel and drops, which is favorable for the formation of superhydrophobic surfaces. The microstructure increased the surface roughness and decreased surface wetting, causing CA to approach 150°. Inspired by the added lotus effect, a stainless-steel substrate with micro–nano structures was fabricated by further chemical etching step in Fig. 2f. Nano pits of approximately 200 nm were formed on the micro structure. This micro–nano composite structure changed morphology of stainless steel surface and increased surface roughness, thus making the stainless-steel surface superhydrophobic.

Experiments showed that surface chemical modification and surface morphology are two key factors in the manufacture of superhydrophobic surfaces [24]. The basic mechanism of superhydrophobicity is that rough surfaces could trap air in the surface of the cave to form a gas film to prevent water from directly contacting the solid matrix [25]. After PFDTES treatments, our stainless-steel surfaces exhibited superhydrophobic properties. The enhanced superhydrophobic performance is attributed to hierarchical roughness forming with fine nano pits standing on micron pore structure, which was similar to the lotus leaf surface [26]. A water droplet that falls on a lotus leaf can easily roll off and take away the adherent dirt particles. The complementary role of micropapillae and hydrophobic wax on the lotus leaf keeps the droplet at a CA of about 160^{o}. This phenomenon is called "lotus effect" [27]. We mimicked the micro–nano structures of the lotus leaf surface by introducing two chemical etching steps and applied the copied superhydrophobicity surface to increase the anti-corrosion of stainless steel. As shown in Fig. 2c, the CA of our superhydrophobic stainless steel was up to 173^{o}, which was slightly higher than the reported values [28,29].

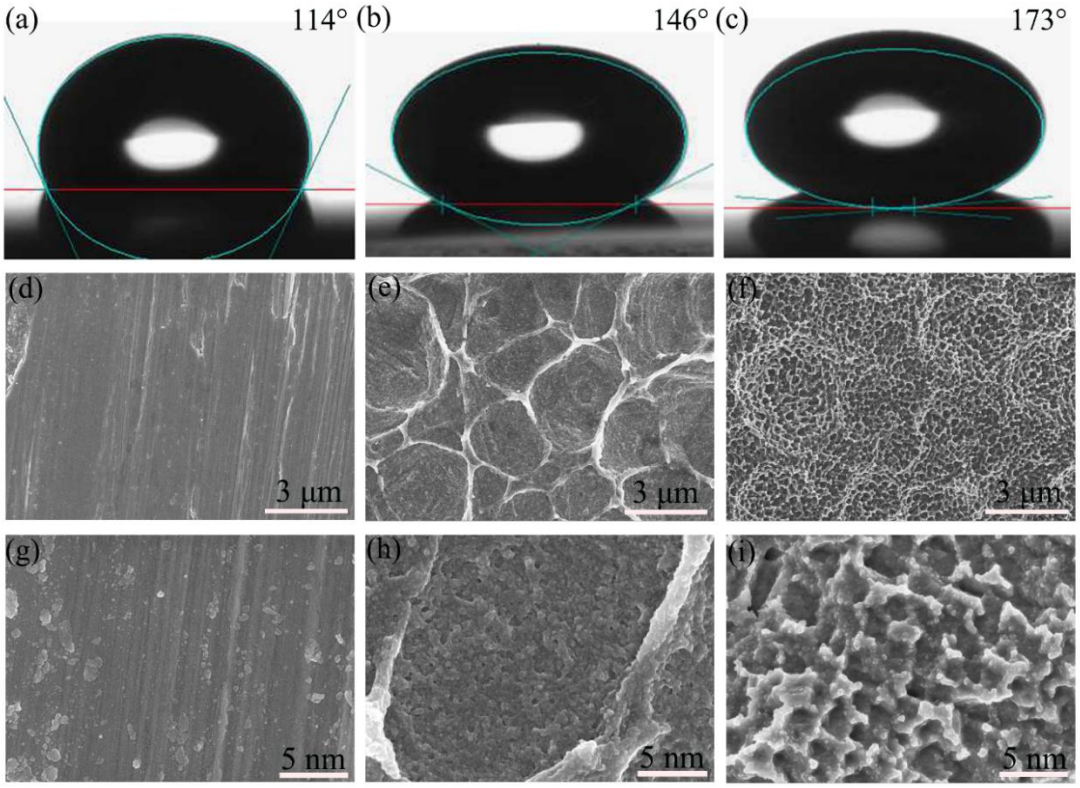

Figure 2. CA test after PFDTES assembling: (a) common stainless steel substrate (b) $FeCl_3$-treated stainless steel surface with micro pore structures (2~5 μm) (c) $FeCl_3$ and HCl-treated stainless steel surface with micro-nano structures; (d), (e) and (f) is corresponding SEM images of (a), (b) and (c); (g), (h) and (i) are magnification images of (d), (e) and (f).

To determine the effect of the etching reaction on the surface crystal structure, we characterized the samples using X-ray diffraction, as shown in Fig. 3a. Evidently, the (111), (200), and (220) peaks corresponded to the crystal diffraction peaks of Fe, indicating that etching did not change the crystal

structure of Fe. Therefore, the crystal structure is not the cause of surface hydrophobicity. However, the intensity of the signal peak (111) changed with increased etching depth, indicating that the etching procedure by $FeCl_3$ and HCl was carried out through the (111) crystal face.

The stainless steel surface changed after etching and modification by using $FeCl_3$, HCl and PFDTES. For understanding the different absorption regions of stainless steel, the as-prepared samples were characterized by DRS in Fig. 3b. The superhydrophobic stainless steel exhibited the lowest reflectivity of all samples in the 350–950 nm wavelength range, demonstrating the strongest antireflection properties. The surface produced uniform distribution of the pore diameters within 2–5 μm after etching by $FeCl_3$, decreasing the reflectivity of the surface, and the decrease range was about 15%. After the second etching step using HCl, numerous pits with a diameter of 200 nm were distributed on the surface with micro pore structures, increasing the complexity of the surface structure and resulting in a lower surface reflectance and a decrease of about 20%. According to the equivalent medium theory, the micro–nano hierarchical structures are equivalent to a dielectric layer in which reflection coefficient changes in gradient. Therefore, the surface showed superior antireflection performance.

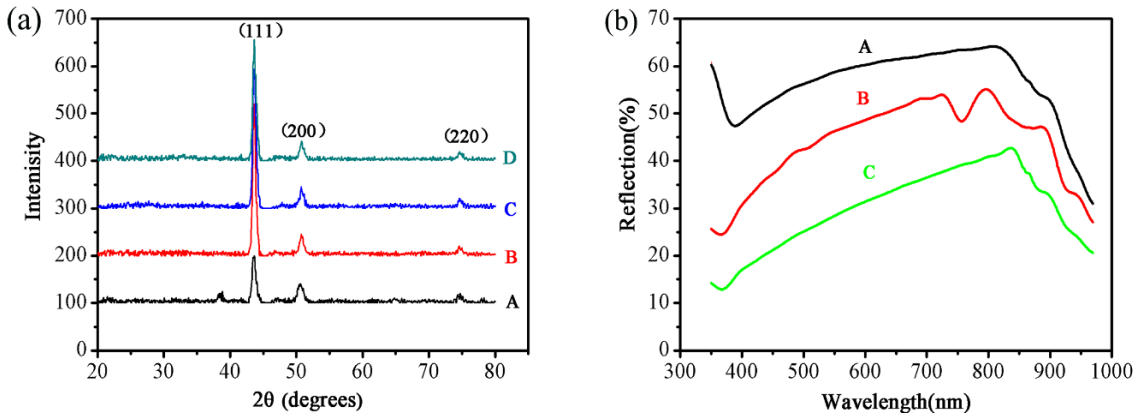

Figure 3. (a) XRD of different substrates: A is common stainless steel substrate; B is stainless steel substrate with micro pore structures; C is stainless steel substrate with micro-nano structures; D is C substrate with PFDTES assembling to fabricate superhydrophobic steel surbstrate. (b) DRS measurement with PFDTES assembling: A is common stainless steel; B is stainless steel substrate with micro pore structures; C is stainless steel substrate with micro-nano structures.

The photograph in Fig. 4a shows that the water droplets appear like balls on the superhydrophobic stainless steel surface. Repeatability test results confirmed good repeatability in preparing superhydrophobic stainless steel surface. CA test after six repeated times yielded 167° at minimum, as shown in Fig. 4b. The stability of the superhydrophobic stainless steel surface is an important evaluation standard of superhydrophobic performance. The prepared superhydrophobic stainless steel sheet was exposed to air for two months; the superhydrophobic performance was virtually unchanged, indicating high stability.

The superhydrophobic properties of stainless steel are related to surface energy. Fig. 2 shows that the superhydrophobic stainless steel surfaces present higher CA than the common stainless-steel surfaces, indicating that the superhydrophobic stainless steel possesses lower surface energies and a stable surface. This finding is in good agreement with electrochemical corrosion test. Fig. 4c displays the polarization curve with different CAs, which were measured in 3.5 wt.% NaCl solution. The corresponding corrosion parameters are summarized in Table 1. The I_{corr} and E_{corr} can be calculated from Tafel extrapolation. R_p values were calculated using the equation [30,31]:

$$R_p = \frac{\beta_a \cdot \beta_c}{2.303 \times I_{corr}(\beta_a + \beta_c)} \quad (1)$$

where β_a and β_c represent the Tafel slopes ($\Delta E/\Delta \log j$) of the anode and cathode, respectively.

In the potentiodynamic polarization curve, higher E_{corr} and lower I_{corr} demonstrate good R_p [32]. The corrosion potential increased from −725 mV for the common stainless-steel surface to −425 mV for a superhydrophobic stainless steel surface. The higher corrosion potential indicates higher R_p because corrosion reactions could only occur when the potential exceeds the corrosion potential [33]. The cathode reaction in the polarization curves corresponds to the hydrogen evolution reaction, and the anodic polarization curve shows the important features related to the corrosion rate of stainless steel [34]. The Tafel slope (β_c) of superhydrophobic stainless steel was not related to the corrosion of stainless steel because hydrogen evolution reaction occurred on the steel. However, the Tafel slope (β_a) of superhydrophobic stainless steel was higher than that of common stainless steel. This finding means that the superhydrophobic stainless steel shows higher overpotential at the same corrosion current and corrosion potential compared with common stainless steel. Therefore, superhydrophobic stainless steel is harder to be corroded compared with common stainless steel. The corrosion rate is linearly proportional to corrosion current density [35]. The I_{corr} of superhydrophobic stainless steel surface is 3.98×10^{-7} A/cm^2, which is the lowest among all the samples, exhibiting a decrease by two orders of magnitude compared with that of common stainless steel (1.77×10^{-5} A/cm^2). Table 1 shows the markedly higher R_p of superhydrophobic surface compared with that of common stainless steel by a factor of 28.9 according to electrochemical corrosion test. The fabricated superhydrophobic stainless steel exhibits 7.5 times higher R_p than the reported superhydrophobic Ni surface [36].

Table 1. CA, E_{corr}, I_{corr}, and R_p of different samples.

CA (°)	E_{corr} (mV)	I_{corr} (mA/cm^2)	R_p (kΩ•cm^2)	β_a (V/dec)	β_c (V/dec)
114	-725	1.77×10^{-5}	0.42	0.036	0.033
146	-605	2.51×10^{-6}	5.08	0.055	0.063
173	-425	3.98×10^{-7}	12.12	0.075	0.017

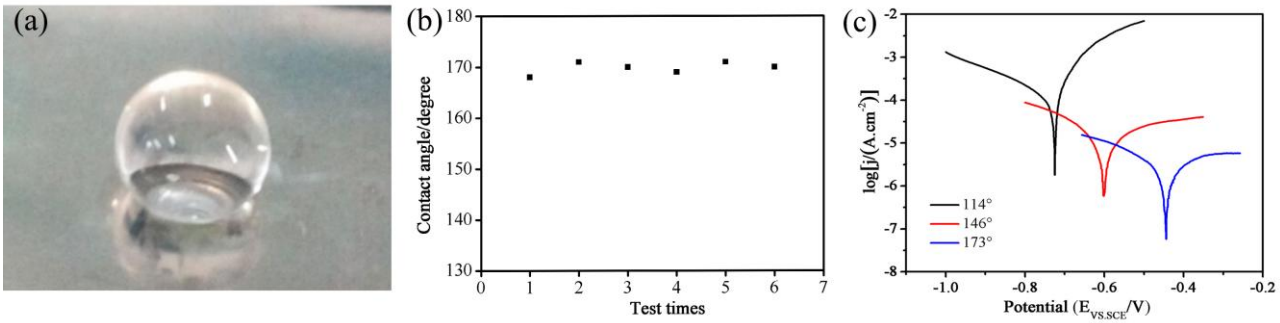

Figure 4. (a) photograph of water droplet on superhydrophobic stainless steel. (b) The superhydrophobic repeatability test of this two steps etching method. (c) Potentiodynamic polarization curves for the stainless steels with different CAs in 3.5 wt.% NaCl solution (Test sensitivity is set to 10^{-2} with a scan rate of 1 mV/s).

4. CONCLUSIONS

In this paper, we developed a superhydrophobic surface on stainless steel for anti-corrosion by using a bioinspired method. Two chemical etching steps have been applied to fabricate the bioinspired micro–nano structures. The CA of the prepared superhydrophobic surface reaches a high value of 173°. The repeatability test demonstrated the stability of this method for fabricating superhydrophobic stainless steel. The prepared superhydrophobic stainless steel surface exhibited high hydrophobicity stability and R_p. Particularly, the bioinspired superhydrophobic stainless steel surface possesses a R_p than is 28.9 times higher than that of common stainless-steel surface.

ACKNOWLEDGEMENTS
The authors thank the financial support of this work by the Startup Project of the Introduce talents research of Dalian University of Technology (No. DUT16QY04).

SUPPORTING INFORMATION:

The reaction rate of etching stainless steel was affected by experimental conditions directly in the process of preparing superhydrophobic surface. The effects of etching time and concentration on the CA were studied in detail.

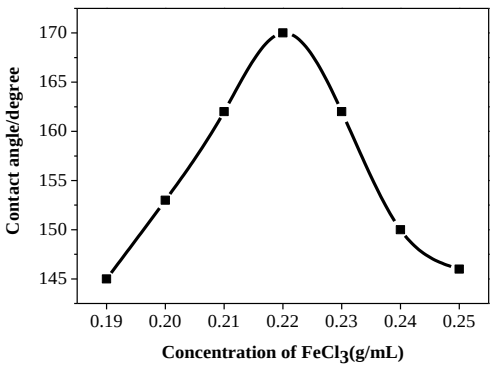

Fig. S1 CA test of stainless steel surface etching with different concentration of $FeCl_3$. The other condition: All the samples are etched for 4 min in $FeCl_3$ etching solution and 20 min in HCl acid solution (1 M). Then, the samples are modified with low-surface-energy molecules of PDFTES.

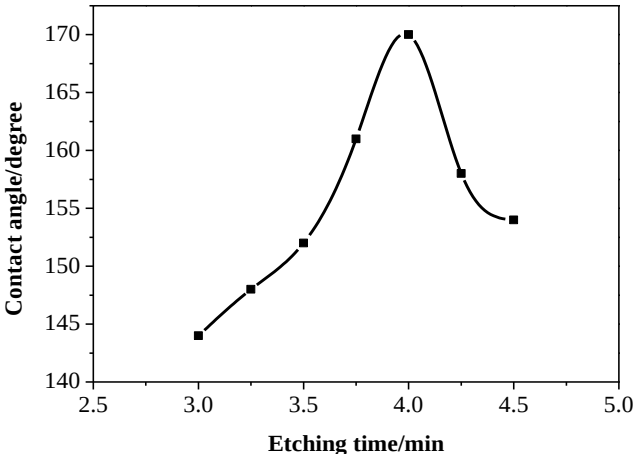

Fig. S2 CA test of stainless steel surface etching with different time in $FeCl_3$ solution. The other condition: The concentration of $FeCl_3$ etching solution is 0.22 g/mL. Then, all the samples are etched for 20 min in HCl acid solution (1 M) and modified with low-surface-energy molecules of PDFTES.

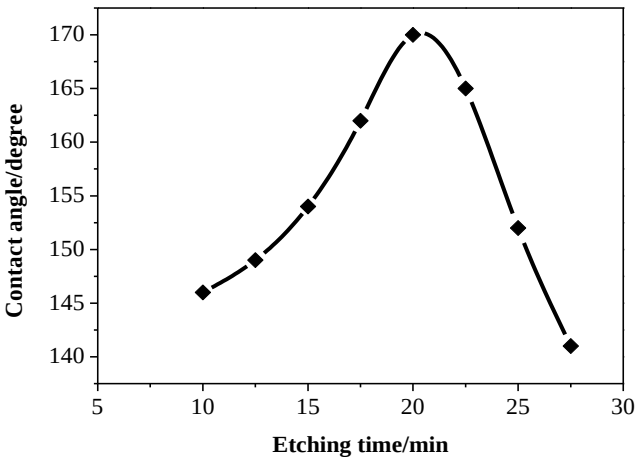

Fig. S3 CA test of stainless steel surface etching with different time in HCl acid solution. The other condition: All the samples are etched for 4 min in $FeCl_3$ etching solution (0.22 g/mL). The concentration of HCl acid solution is 1 M. Then, the samples are modified with low-surface-energy molecules of PDFTES.

References

1. W. Barthlott, and C. Neinhuis, *Planta*, 202 (1997) 1.
2. C. Neinhuis, and W. Barthlott, *Ann. Bot.*, 79 (1997) 667.
3. L. Feng, Y. Zhang, J. Xi, Y. Zhu, N. Wang, F. Xia, and L. Jiang, *Langmuir*, 24 (2008) 4114.
4. J. Xi, and L. Jiang, *Ind. Eng. Chem. Res.*, 47 (2008) 6354.
5. N. Zhang, S. Lu, W. Xu, and Y. Zhang, *New J. Chem.*, 38 (2014) 4534.
6. S. Sethi, L. Ge, L. Ci, P. M. Ajayan, and A. Dhinojwala, *Nano Lett.*, 8 (2008) 822.
7. M. P. Sousa, and J. F. Mano, *Cellulose*, 20 (2013) 2185.
8. A. M. Costa, M. Alatorre-Meda, C. Alvarez-Lorenzo, and J. F. Mano, *Small*, 11 (2015) 3648.
9. N. Wang, Y. Lu, D. Xiong, C. J. Carmalt, and I. P. Parkin, *J.Mater. Chem. A*, 4 (2016) 4107.
10. C. Du, J. Wang, Z. Chen, and D. Chen, *Appl. Surf. Sci.*, 313 (2014) 304.
11. F. Wang, S. Yu, M. Xue, J. Ou, and W. Li, *New J. Chem.*, 38 (2014) 4388.
12. Y. T. Cheng, D. E. Rodak, C. A. Wong, and C. A. Hayden, *Nanotechnology*, 17 (2006) 1359.

13. X. Zhang, Y. Song, and X. Wang. *Int. J. Electrochem. Sci.*, 12 (2017) 32.
14. C. Mo, Y. Zheng, and F. Wang, *Int. J. Electrochem. Sci.*, 10 (2015) 7380.
15. H. F. Guo, G. P. Li, L. Cheng, J. W. Zhou, W. L. Liu, Z. H. Zhang, C. M. Li, X. D. Dai, W. C. Chang, F. J. Yang, and C. Liu, *Int. J. Electrochem. Sci.*, 8 (2013) 11278.
16. S. Lyu, D. C. Nguyen, D. Kim, W. H. Wang, and B. Yoon, *Appl. Surf. Sci.*, 286 (2013) 206.
17. T. Tatsuma, S. Saitoh, Y. Ohko, and A. Fujishima, *Chem. Mater.*, 13 (2001) 2838.
18. H. Wang, and R. Akid, *Corros. Sci.*, 49 (2007) 4491.
19. A. Conde, M. A. Arenas, A. De Frutos, and J. De Damborenea, *Electrochim. Acta.*, 53 (2008) 7760.
20. L. M. Palomino, P. H. Suegama, I. V. Aoki, M. F. Montemor, and H. G. De Melo, *Corros. Sci.*, 51 (2009) 1238.
21. W. Trabelsi, L. Dhouibi, E. Triki, M. Ferreira, and M. F. Montemor, *Surf. Coat. Technol.*, 192 (2005) 284.
22. S. Mayavan, T. Siva, and S. Sathiyanarayanan, *RSC Adv.*, 3 (2013) 24868.
23. M. A. Deyab, *J. Power Sources*, 268 (2014) 50.
24. N. J. Yu, Y. F. Yu, Y. F. Li, S. P. Song, S. B. Huo, and X. Y. Han, *Surf. Rev. Lett.*, 17 (2010) 375.
25. Y. Yan, N. Gao, W. Barthlott, *Adv. Colloid Interface Sci.*, 169 (2011) 80.
26. L. Feng, S. H. Li, Y. S. Li, H. J. Li, L. J. Zhang, J. Zhai, Y. L. Song, B. Q. Liu, L. Jiang, and D. B. Zhu, *Adv. Mater.*, 14 (2002) 1857.
27. K. S. Liu, X. Yao, and L. Jiang, *Chem. Soc. Rev.*, 39 (2010) 3240.
28. T. Wu, Y. Pan, and L. Li, *J. Colloid Interface Sci.*, 348 (2010) 265.
29. Y. Lee, S. H. Park, K. B. Kim, and J. K. Lee, *Adv. Mater.*, 19 (2007) 2330.
30. H. Duan, C. Yan and F. Wang, *Electrochim. Acta*, 52 (2007) 3785.
31. W. Xu, J. Song, J. Sun, Y. Lu, and Z. Yu, *ACS Appl. Mater. Interfaces*, 3 (2011) 4404.
32. R. O. Hussein, D. O. Northwood and X. Nie, *J. Alloys Compd.*, 541 (2012) 41.
33. C. Vasilescu, S. Drob, E. Neacsu, J.M. Rosca, *Corros. Sci.*, 65 (2012) 431.
34. T. Zhang, X. Liu, Y. Shao, G. Meng and F. Wang, *Corros. Sci.*, 50 (2008) 3500.
35. C.-c. Li, X.-y. Guo, S. Shen, P. Song, T. Xu, Y. Wen, H.-F. Yang, *Corros. Sci.*, 83 (2014) 147.
36. J. Tan, J. Hao, Z. An, C. Liu, *Int. J. Electrochem. Sci.*, 12 (2017) 40.